Lithographic characterization of the flare in the Berkeley 0.3 numerical aperture extreme ultraviolet microfield optic

Jason P. Cain[a)]
Department of Electrical Engineering and Computer Sciences, University of California, Berkeley, California 94720

Patrick P. Naulleau
College of Nanoscale Science and Engineering, University of Albany, New York 12203

Eric M. Gullikson
Center for X-Ray Optics, Lawrence Berkeley National Laboratory, Berkeley, California 94720

Costas J. Spanos
Department of Electrical Engineering and Computer Sciences, University of California, Berkeley, California 94720

(Received 20 January 2006; accepted 15 March 2006; published 24 April 2006)

Flare remains a crucial issue for extreme ultraviolet (EUV) lithography. Achieving required flare levels demands mid-spatial-frequency surface roughness levels on the order of 1 Å, which is on par with present metrology limits. Lithographic verification of predicted flare levels is thus critical to the validation of current metrology methods. In this work we present the lithographic characterization of flare in the Berkeley EUV microfield exposure tool. Experimental analysis shows good agreement between predicted and measured results. The results also show that it is essential to compensate for proximity and die-to-die effects. In an isolated microfield, flare values of 6.8% and 4.8% in 500 nm and 2 μm lines, respectively, have been verified. © *2006 American Vacuum Society.*
[DOI: 10.1116/1.2194946]

I. INTRODUCTION

One of the technology-specific challenges still facing extreme ultraviolet (EUV) lithography is flare. In the EUV regime, flare is dominated by nonspecular reflection (scatter) from the imaging mirrors themselves. The problem is accentuated due to the reflective nature of the optics as well as the extremely short wavelength used (13.5 nm). Of most concern for flare are those spatial frequencies lying above the figure-error regime (typically characterized by Zernike polynomials) yet low enough to cause the scattered light to remain within the imaging field. This scattered light is referred to as flare and detrimentally impacts the aerial-image contrast. The spatial frequency range of relevance to flare, typically referred to as mid-spatial-frequencies, nominally falls in the 1 mm^{-1}–1 μm^{-1} range. Achieving target flare levels requires the mid-spatial-frequency roughness to approach 1 Å, on par with present metrology limits. Lithographic verification of predicted flare levels is thus critical to the validation of current metrology methods. Here we present the lithographic characterization of flare in the Berkeley EUV microfield exposure tool. Experimental analysis shows good agreement between predicted and measured results. The results also show that it is essential to compensate for proximity and die-to-die effects when lithographically characterizing the intrinsic flare. In an isolated microfield, flare values of 6.8% and 4.7% in 500 nm and 2 μm lines, respectively, have been verified.

II. FLARE MODELING

The fact that the flare in EUV systems is dominated by surface scatter from the imaging mirrors themselves makes prediction of flare relatively straightforward as compared to deep ultraviolet (DUV) systems. This is because DUV systems can suffer from a variety of factors including hard to quantify effects such as spurious and multiple reflections. A key metric in the prediction of flare for EUV systems is the total integrated scatter (TIS) of the imaging optics defined as the ratio of the nonspecular scattered power to the reflected specular power when light is incident on a surface. The TIS is given by[1]

$$\mathrm{TIS} = \frac{P_s}{P_0} \cong \left(\frac{4\pi\sigma_s \cos\theta_i}{\lambda} \right)^2, \quad (1)$$

where P_s is scattered power, P_0 is specular reflected power, σ_s is the standard deviation of the surface roughness, θ_i is the angle of incidence, and λ is the wavelength of light. As Eq. (1) shows, TIS is proportional to $1/\lambda^2$, hence a significant issue for EUV where the wavelength is only 13.5 nm.

The TIS represents the flare in an infinitely large field, but in practice we are concerned only with a limited field size, thus we only need to consider roughness periods leading to scatter within the field of view. The field integrated scatter (FIS) is defined as

$$\mathrm{FIS}(r) \cong \left(\frac{4\pi\sigma_s(r)\cos\theta_i}{\lambda} \right)^2, \quad (2)$$

where r is the field radius and $\sigma_s(r)$ is the standard deviation of the surface roughness including frequencies causing

a)Electronic mail: jason.cain@amd.com

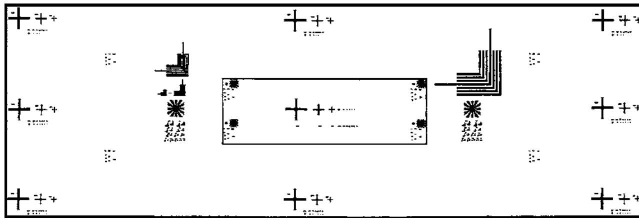

FIG. 1. Schematic diagram of the flare-measurement pattern. The cross patterns are replicated at various points in the field in order to probe the field dependence of the flare. Crosses are used in order to characterize flare anisotropy. The pattern includes features ranging from 2 μm in width down to 30 nm.

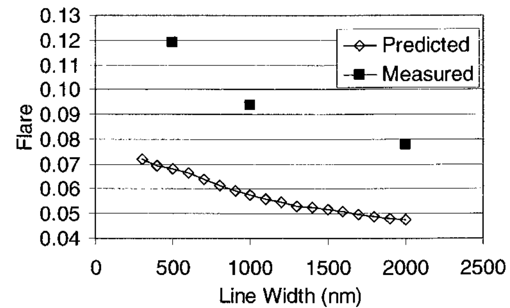

FIG. 2. Measured vs predicted flare as a function of feature size for isolated dark lines in a bright field. Measurement includes correction for imperfect mask contrast.

image-plane displacements up to a radius r. Flare for any given feature size (r_d) within any given field size (r_b) is thus

$$\text{Flare}(r_d, r_b) = \text{FIS}(r_b) - \text{FIS}(r_d). \quad (3)$$

In practice, the data we have to work with for describing the rough surface is the power spectral density (PSD) of the roughness. To get from the PSD to the surface roughness we can use the relation

$$\sigma_s(r) = \sqrt{\int_0^{\sin(\tan^{-1}(r/d_i))/\lambda} \text{PSD}(f) 2\pi f df}, \quad (4)$$

where d_i is the distance from the rough surface to the image plane.

III. LITHOGRAPHIC MEASUREMENT OF FLARE

The flare in the Berkeley EUV microfield exposure tool[2] was measured using a lithographic technique derived from Kirk's method.[3] This method has been used to characterize other EUV optics[4] and employs simple cross patterns of varying size placed in an otherwise bright field. The full field layout for the flare experiment is shown in Fig. 1. The cross patterns are replicated at various points in the field in order to probe the field dependence of the flare and crosses are used to characterize the anisotropy of the flare. The pattern includes features ranging from 2 μm in width down to 30 nm.

The experiment involves printing the pattern from Fig. 1 over an extremely large dose range with relatively fine steps. On the low side we must go below dose to clear for the large open regions (or E_0) and on the high dose side we must go above the dose required to completely clear the dark regions in the largest features of interest (2 μm in our case). For example, if an optic has a flare of 5%, then the high dose will need to be at least 20 times E_0. To optimize the precision of the measurement while minimizing the total number of exposures, exponential dose steps should be used instead of linear. Exponential steps guarantee the relative dose step sizes to be the same at the top and bottom of the entire range. For the data presented here we used an exponential dose step size of 5%, leading to a flare-measurement precision of 1% absolute.

The exposures were done in a 125 nm thick layer of Rohm and Haas *EUV-2D* photoresist, and both postapplication and postexposure bakes were performed at 130 °C. The illumination conditions were annular with $\sigma_{\text{inner}}=0.3$ and $\sigma_{\text{outer}}=0.7$, typical operating conditions for this optic. Flare for a given feature size is then measured from the exposures by dividing the exposure dose required to clear the resist in the bright region (E_0) by the dose to clear in the dark regions (E_{dark}):

$$\%\text{Flare} = \frac{E_0}{E_{\text{dark}}} \times 100. \quad (5)$$

Figure 2 shows the measured flare compared to the predicted flare for the optical system alone. A very large discrepancy is evident. We see both a magnitude error of approximately a factor of 2 as well as a slope error. The impact of nonideal mask contrast is already compensated for in the data shown in Fig. 2. Separate measurements have shown the absorber regions to reflect 1% of the light relative to the clear regions (mask contrast of 98%) leading to an effective flare of 1% that must be compensated for when comparing the measurement to the predicted flare of the optical system.

To address the large discrepancy evident in Fig. 2 we begin by considering proximity or resolution-limit effects. It is evident that even in the ideal zero-flare case the dark regions on the mask will not image as completely dark due to the limited resolution of the optic. This effect becomes increasingly important as the feature size is decreased. Figure 3

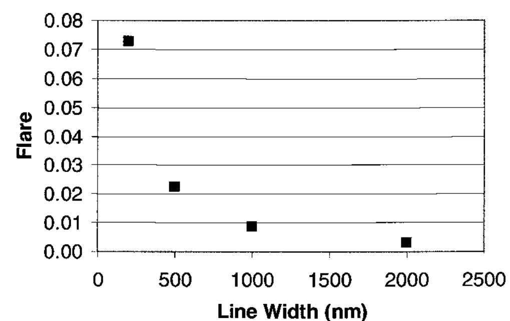

FIG. 3. Calculated effective flare from a scatter-free system. The calculations include the full measured wave front of the system as well as the actual illumination conditions. The model also includes the microfield optic central obscuration having a radius of 30% of the full numerical aperture of the system.

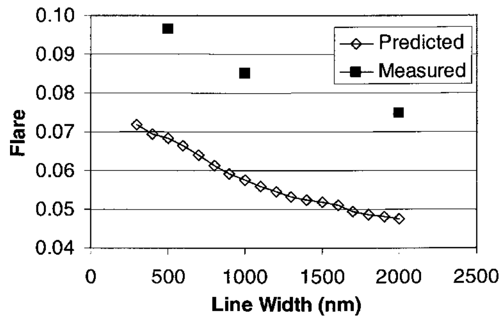

FIG. 4. Measured vs predicted flare after correction for the resolution-limit effects. The agreement of the slope is much improved; however, the large offset persists.

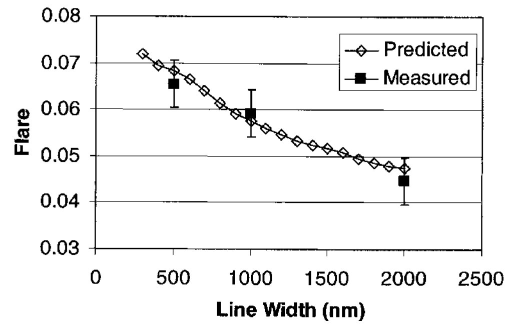

FIG. 6. Measured vs predicted flare after experimental mitigation of the die-to-die effects and correction for the mask contrast and the resolution-limit effects.

shows the PROLITH (Ref. 5) calculated effective flare for a scatter-free system. The calculations include the full measured wave front of the system[6–8] as well as the actual illumination conditions. The model also includes the optic's central obscuration having a radius of 30% of the full numerical aperture of the system. The results show that although resolution-limit effects have virtually no impact on 2 μm features, they become quite important at feature sizes of 500 nm and below. At 500 nm, we see an effective flare of 2%. Although the resolution-limit effect does not explain the large absolute discrepancy, it does account for the observed slope error in Fig. 2. Figure 4 shows the measurement after compensation for the effect in Fig. 3.

The next effect we consider is flare from adjacent die. In practice a very large number of exposures are required to encompass the entire dose range needed for the flare experiment and in fine enough steps. Moreover, in order to mitigate any focus error effects, the wafer included replicas of the through dose range at various focus settings. These conditions led to a total of approximately 1000 exposure fields on the wafer packed into a 12×12 mm^2 region with 80% fill factor. It is evident that this is significantly different than the ideal case of a single 200×600 μm^2 exposure as assumed in the flare prediction. Figure 5 shows the predicted flare in a 500 nm round contact as a function of field diameter. Long-range flare is seen to have a significant impact and could easily be responsible for the factor-of-2 discrepancy seen in Fig. 2. An exact computation of the experimental condition is rather complicated due to the incomplete fill factor and the fact that the exposure dose varies by well over an order of magnitude over the series of exposures used in the flare experiment.

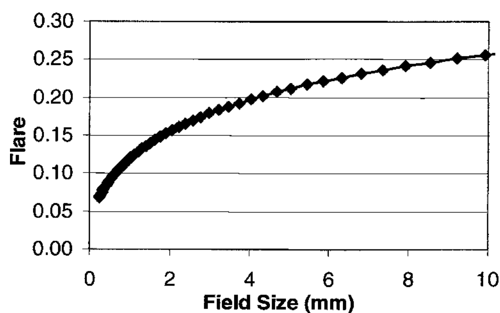

FIG. 5. Predicted flare in a 500 nm round contact as a function of field diameter. Long-range flare is seen to have a significant impact and could easily be responsible for the factor-of-2 discrepancy seen in Fig. 2. An exact computation of the experimental condition is rather complicated due to the incomplete fill factor and the fact that the exposure dose varies by well over an order of magnitude over the series of exposures used in the flare experiment.

Instead of performing the rigorous flare computation to match the experimental conditions, we modify the experimental conditions to render adjacent die effects negligible. This is achieved by reducing the total number of exposures by a factor of 4 and by reducing the fill factor. In this new condition, the total exposed region is 8×8 mm^2 with a 45% fill factor. This was achieved by reducing the number of focus steps and by eliminating the doses in the range near dose to size (those doses are irrelevant to the measurement of flare). The new measurement results after correction for the mask contrast and the resolution-limit effects are shown in Fig. 6. Here we see excellent agreement between predicted and measured flare. The error bars are determined based on the experimental dose step size.

IV. SUMMARY

The lithographic characterization of flare in the Berkeley EUV microfield exposure tool has been presented. The results show that it is essential to compensate for proximity and die-to-die effects. It is preferable to maximize the die-to-die spacing to minimize the effects of adjacent fields; however, this requirement must be balanced against the need to fit a large number of fields on the wafer in order to cover the large range of exposure dose with sufficient precision. Moreover, it is not recommended to try to characterize flare in features smaller than 500 nm due to the significance of proximity effects in that regime. Minimizing the flare from adjacent die and compensating for proximity and mask contrast effects, experimental results are in excellent agreement with prediction. In an isolated microfield, flare values of 6.8% and 4.8% in 500 nm and 2 μm lines, respectively, have been verified. Also we note that to within our measurement uncertainty of approximately 1% absolute flare, we saw no appreciable within-field location dependence or anisotropy in the flare.

ACKNOWLEDGMENTS

The authors are greatly indebted to Paul Denham, Ken Goldberg, and Brian Hoef for expert support with the exposure tool. The authors would also like to thank Robert Brainard and Thomas Koehler of Rohm and Haas for resist and process support and Kim Dean of SEMATECH for programmatic support. This research was performed at Lawrence Berkeley National Laboratory and supported by SEMATECH. Additional support was provided by funding from Advanced Micro Devices, Applied Materials, Atmel, Cadence, Canon, Cymer, DuPont, Ebara, Intel, KLA-Tencor, Mentor Graphics, Nikon Research, Novellus Systems, Panoramic Technologies, Photronics, Synopsis, Tokyo Electron, and the UC Discovery Grant. Lawrence Berkeley National Laboratory is operated under the auspices of the Director, Office of Science, Office of Basic Energy Science, of the U.S. Department of Energy.

[1]J. C. Stover, *Optical Scattering Measurement and Analysis*, 2nd ed. (SPIE, Bellingham, WA, 1995).
[2]P. Naulleau *et al.*, J. Vac. Sci. Technol. B **22**, 2962 (2004).
[3]J. P. Kirk, Proc. SPIE **2197**, 566 (1994).
[4]S. H. Lee, P. Naulleau, C. Krautschik, M. Chandhok, H. N. Chapman, D. J. O'Connell, and M. Goldstein, Proc. SPIE **5037**, 103 (2003).
[5]PROLITH is a registered trademark of KLA-Tencor Corporation, 160 Rio Robles, San Jose, California 95134.
[6]K. Goldberg, P. Naulleau, P. Denham, S. Rekawa, K. Jackson, E. Anderson, and J. Liddle, J. Vac. Sci. Technol. B **22**, 2956 (2004).
[7]P. Naulleau, J. Cain, and K. Goldberg, J. Vac. Sci. Technol. B (to be published).
[8]P. Naulleau, J. Cain, and K. Goldberg, Appl. Opt. **45**, 1957 (2006).